CrossMark

Facile and green synthesis of core–shell ZnSe/ZnS quantum dots in aqueous solution

S. L. Zhang[1] · C. F. Lin[1] · Y. L. Weng[1] · L. C. He[1] · T. L. Guo[1] · Y. A. Zhang[1] · X. T. Zhou[1]

Abstract

In this work, core–shell ZnSe/ZnS quantum dots (QDs) with excellent blue light emission were successfully synthesized in aqueous solution using thioglycolic acid as a stabilizer, thiourea as a sulphur source, and zinc acetate dihydrate as a Zn source. The crystal structure and optical properties of the as-synthesized ZnSe/ZnS QDs were characterized using X-ray diffraction, transmission electron microscopy, X-ray photoelectron spectroscopy, Fourier transform infrared spectroscopy, photoluminescence (PL) and UV–Visible spectroscopy. The ZnSe/ZnS QDs had a cubic zinc blende crystalline structure with an average particle size of approximately 4.6 nm. The excitonic emission slightly shifted to a longer wavelength and the PL intensity increased considerably with the growth of the ZnS shells. Meanwhile, the PL quantum yield of the ZnSe/ZnS QDs increased to 58.5%, which was much higher than that of ZnSe QDs. The exciton radiative lifetimes were approximately 46.3 and 23.1 ns for the core–shell ZnSe/ZnS QDs and ZnSe QDs, respectively.

1 Introduction

II–VI semiconductor nanocrystals, known as quantum dots (QDs), are interesting materials due to their excellent electronic and optoelectronic properties. These materials have been developed for a wide range of potential applications, such as LEDs [1, 2], lasers [3], solar cells [4], thin films transistors [5], field emitters [6], and biomedicine [7]. Among the various II–VI QDs, cadmium compounds, including CdSe, CdTe and alloyed QDs, are toxic and dangerous for the human body and the environment; therefore, lower toxic zinc compounds have attracted much interest [6, 8, 9]. Zinc selenide (ZnSe) has a wide band-gap (2.7 eV) and large exciton binding energy (21 meV) at room temperature [10, 11]. In comparison with cadmium compounds, ZnSe with little toxicity is suitable for practical applications [12–14]. In recent decades, many groups have synthesized ZnSe QDs using different methods. For example, Molaei et al. synthesized ZnSe QDs with an average size of 3 nm using a microwave irradiation method. The excitonic and trap state emissions are located at approximately 415 and 500 nm, respectively [15]. Ehsan et al. used a facile method to synthesize ZnSe QDs in an aqueous media. The ZnSe QDs with an average size of 4.6 nm had a deep-blue luminescence, and their band edge and trap emission are located at 370 and 460 nm, respectively [16]. Wang et al. presented a novel cationic inverse injection method to synthesize ZnSe QDs with a bright blue luminescence in an aqueous media [17].

Additionally, compared to another popular II–VI material, zinc sulphide (ZnS) with a large band-gap energy (3.66 eV) has outstanding photoelectric and luminescent properties with extensive applications [18]. Thus, the growth of a ZnS shell around ZnSe QDs could improve its optical properties and decrease its toxicity. The development of novel methods for the synthesis of core–shell ZnSe/ZnS nanostructures have been the subject of intensive investigation in recent years. For example, Lin et al. synthesized ZnSe/ZnS core/shell NCs with strong photoluminescence (PL) intensity at 150 °C for 6 h. The wide band-edge emission was centered at 476 nm [19]. Li et al. reported a self-assembled method to synthesize ZnSe/ZnS/L-Cys quantum dots synthesized at room temperature or at a reflux temperature of 90 °C for 3 h [20]. Molaei et al. reported the synthesis of ZnSe and core–shell ZnSe/ZnS NCs using a rapid and room temperature photochemical method. The PL spectra indicated a broad emission with two peaks located about 370 and

✉ Y. A. Zhang
yongaizhang@fzu.edu.cn

✉ X. T. Zhou
xtzhou@fzu.edu.cn

1   College of Physics and Information Engineering, University of Fuzhou, Fuzhou 350016, Fujian, China

Springer

490 nm related to band edge and trap state emission, respectively. The excitonic emission of ZnSe/ZnS NCs shifted to a longer wavelength after the growth of ZnS shells [21]. Cao et al. reported a facile, two-step method to synthesize core/shell ZnSe/ZnS QDs with highly luminescent UV-blue emission under mild conditions (low temperatureo150 °C) [22]. Kim et al. employed a microwave-assisted hydrothermal method to prepare highly luminescent ZnSe-based QDs. Their QY was higher than 90% when the ZnS shells were applied to form the ZnSe/ZnS-core/shell structure [23].

Recently, we proposed a cation-inverting-injection method to synthesize ZnSe QDs in an aqueous solution [24]. Here, we improved this method to synthesize high-quality core/shell ZnSe/ZnS QDs using a facile and green route in an aqueous solution. The ZnS shell was epitaxially overgrown around the ZnSe core after the introduction of additional $Zn(OAc)_2$, thioglycolic acid (TGA), and thiourea to the ZnSe reaction solution, where the thiourea acted as a sulphur source (S^{2-}) for the growth of ZnS shells and the TGA acted simultaneously as both the capping agent and a S^{2-} source. Various analysis tools were employed to characterize the crystal structure and optical properties of the as-synthesized core–shell ZnSe/ZnS QDs under optimized conditions. This method is facile and green, and the PL QY of the ZnSe/ZnS QDs were improved.

2 Experimental details

2.1 Materials and reagents

Zinc acetate dihydrate ($Zn(OAc)_2 \cdot 2H_2O$, 99.99%), sodium borohydride ($NaBH_4$, 99.99%), selenium powder (Se, 99.99%), thioglycolic acid (TGA, 99.99%) and thiourea (99.0%) were purchased from Sigma-Aldrich (Shanghai) Trading Limited Company. Sodium hydroxide (NaOH, 96%) and isopropyl alcohol were purchased from Shanghai Guoyao Chemical Reagent Company. All the reagents were of analytical grade and were used without further purification.

2.2 Synthesis of ZnSe QDs

The flow chart of ZnSe/ZnS QDs is shown in Fig. 1. First, the ZnSe QDs were prepared using the cationic inverse injection method in an aqueous solution [24]. Freshly prepared NaHSe solution, as the Se precursor solution, was injected into a three-necked flask after degassing with N_2 for 30 min, where the mixture of TGA had been dispersed into the deionized water and the pH was adjusted to 8.5 with the NaOH solution. Second, a prepared Zn-TGA solution, as the Zn precursor, was slowly injected into the compounded solution and the final feeding ratio of Zn^{2+}:NaHSe:TGA was tuned to 1:0.125:1.2. After heating at 90 °C for 2 h, the
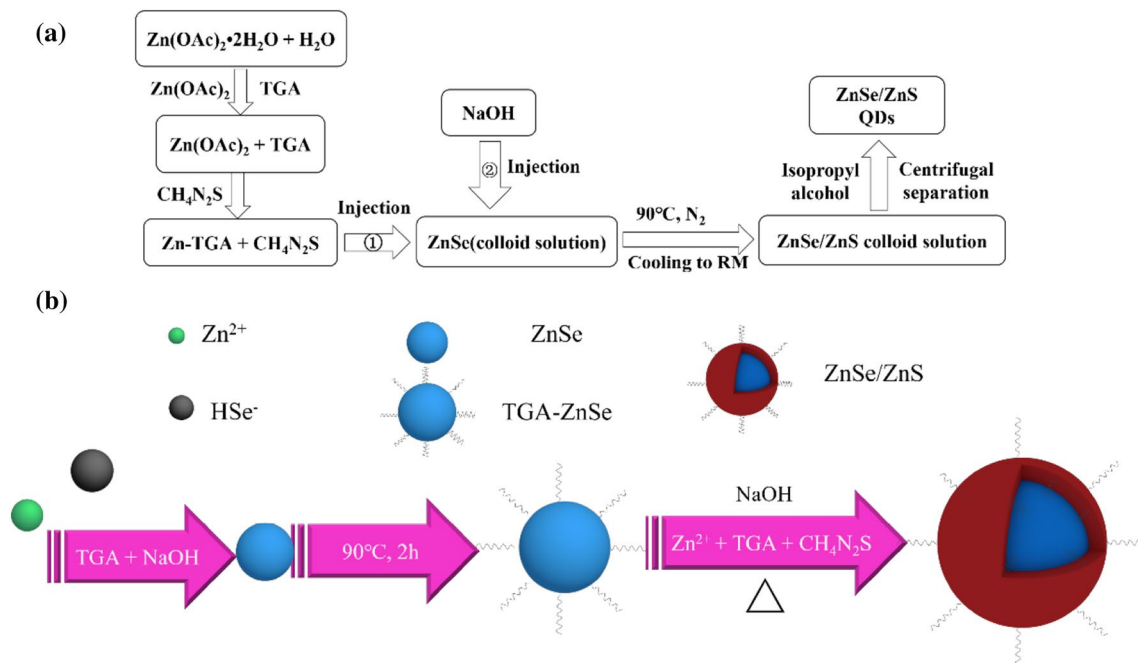
Fig. 1 **a** Flow chart for the synthesis of core–shell ZnSe/ZnS QDs and **b** schematic illustration for the growth of core–shell ZnSe/ZnS QDs

three-necked flask was immediately put into water to cool, and the colloid solution of ZnSe QDs was obtained.

2.3 Synthesis of ZnSe/ZnS QDs

Core/shell ZnSe/ZnS QDs were synthesized using the epitaxial overgrowth method in an aqueous solution. First, $Zn(OAc)_2 \cdot 2H_2O$ (0.1098 g, 0.5 mmol), deionized water (30 ml), TGA (69 μl, 1 mmol) and thiourea (0.038 g, 0.5 mmol) were put into the reaction vessel. The mixed solution was stirred until it was completely dissolved at room temperature. Then, the mixture was injected into the previously prepared ZnSe colloid solution (the molar ratio of ZnSe/thiourea = 1:5), where the pH value was adjusted with the NaOH solution (5 M) and the reaction flask was slowly bubbled with N_2 and was under magnetic stirring during the whole reaction process. The reaction temperature was fixed at 90 °C for 3 h, after rapidly cooling to room temperature, the core/shell ZnSe/ZnS colloid solution was obtained. Finally, the as-synthesized ZnSe/ZnS colloid solution was centrifuged by mixing it with the same volume of isopropanol, and then the precipitate was dispersed in a small amount of ultrapure water. ZnSe/ZnS QDs powder were successfully obtained after drying at 60 °C for 10 h under the vacuum condition.

2.4 Sample characterization

The PL spectra of the as-synthesized ZnSe/ZnS QDs were measured using a F-4600 fluorescence spectrophotometer with a Xe lamp as the excitation source, and the UV–Visible (UV–Vis) absorption spectra were measured using a Shimadzu 3600 UV–Vis near infrared spectrophotometer. The X-ray diffraction (XRD) spectra of the as-synthesized samples were analysed using a Bruker AXS D8-advance X-ray diffractometer with Cu Kα radiation (λ = 1.5418 Å) within the range of 2θ = 10°–80°. The morphology was characterized using transmission electron microscopy (TEM) and high-resolution TEM (HRTEM, Tecnai G2 F20 S-Twin) with an accelerating voltage of 200 kV. The compositions of the as-synthesized samples were characterized using an X-ray photoelectron spectroscopy (XPS) system consisting of a Kratos Axis Ultra X-ray photoelectron spectrometer and a monochromatic Al Kα source (1486.6 eV). The Zeta potential and particle size distribution were measured using a Zeta Potential and Nano Particle Analyzer (NanoPlus 3). The chemical bonds of the ZnSe and ZnSe/ZnS QDs were measured using a Fourier transform infrared spectrometer (FT-IR, Nicolet is50). The fluorescence lifetimes were measured using a FL920-fluorescence lifetime spectrometer (Edinburgh Instruments). The recorded decay curves were fitted with a multiexponential function deconvoluted with the system response.

3 Results and discussion

3.1 The optimization of the synthesis conditions of ZnSe/ZnS QDs

High quality QDs strongly depend on the experimental conditions. To obtain high quality core–shell ZnSe/ZnS QDs, we investigated the effects of a series of experimental variables on the optical performances of the as-synthesized ZnSe/ZnS QDs, including the pH value, the molar ratio of ZnSe/thiourea and refluxing time. The experimental results are shown in Fig. 2.

The pH is an important factor that influences the shell growth and optical performances of ZnSe/ZnS QDs. Figure 2a shows the effect of the pH on the PL spectra of as-synthesized ZnSe/ZnS QDs, where the pH was varied from 8 to 9.5 while the molar ratio of ZnSe/ thiourea was kept at 1:5 and the refluxing time was kept at 3 h. The main contribution of excitonic emission is from the band edge emission and the strongest PL intensity is observed at the pH of 8.5. With the increase of the pH, the PL intensity decreases sharply because of the excessive growth of the ZnS shell, resulting in the aggregation and precipitation of quantum dots. The inset in Fig. 2a shows the PL peaks position of the band edge emission at various pH values. With the increase of the pH, the peak of the band edge emission moves from 398 to 410 nm because the growth rate of ZnS shell increases monotonously. The faster growth rate at a higher pH can attribute to the faster decomposition rate of thiourea and lead to the facile availability of the free sulphur precursor S^{2-}. While at a lower pH, the decomposition product of thiourea exists in the form of H_2S, which requires a deprotonation process before the formation of ZnS shells [25, 26]. Additionally, under alkaline conditions, the deprotonated thiol and carboxy could balance the attractive and repulsive forces and stabilize quantum dots in the aqueous solution, which is beneficial to enhancing the intensity of the PL [27, 28].

Figure 2b reveals the PL spectra of the as-synthesized ZnSe/ZnS QDs and the insets shows the PL peaks position of the band edge emission, where the molar ratio of ZnSe/ thiourea were varied from 1:2 to 1:6 while keeping the pH 8.5 and the refluxing time at 3 h. The best results for the excitation emission peak can be achieved due to the growth of ZnS shells on the surface of the ZnSe cores when the molar ratio of ZnSe/thiourea is 1:5.

Figure 2c presents the effect of the refluxing time on the PL spectra of as-synthesized ZnSe/ZnS QDs, where the molar ratio of ZnSe/thiourea was fixed as 1:5 and the pH was 8.5. The PL intensity is strongest at the refluxing time of 3 h due to the growth of ZnS shells. Meanwhile, the peaks of the band edge emission slightly shift to longer
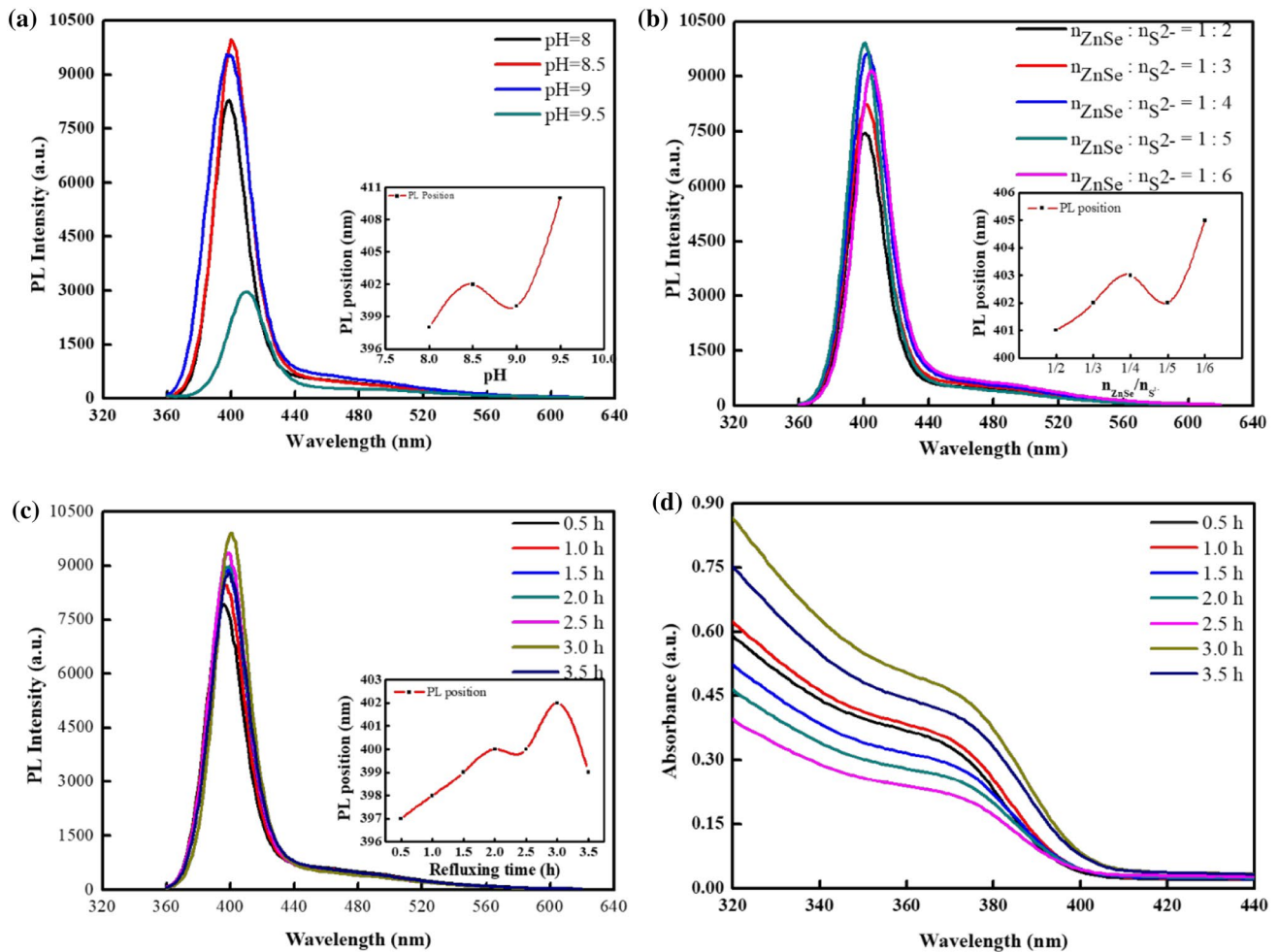
Fig. 2 Optical properties of as-synthesized ZnSe/ZnS QDs: **a** PL spectra at various pH values (Inset: the evolution of the PL peak position versus pH values); **b** PL spectra at various $n_{ZnSe}/n_{thiourea}$ ratios (Inset: the evolution of the PL peak position versus $n_{ZnSe}/n_{thiourea}$ ratios); **c** PL spectra at various refluxing times (Inset: the evolution of the PL peak position versus refluxing times); and **d** UV–Vis absorption spectra at various refluxing times

wavelengths, as shown from the inset in Fig. 2c. During the initial stage of the reaction with the growth of ZnS shells, the surface defects of the ZnSe cores will be inactivated and the surface charge density will be reduced, which results in the enhancement of the fluorescence intensity. However, the core–shell interface forms some defects due to the lattice mismatch between ZnS and ZnSe and introduces non-radiative transition channels as the thickness of ZnS shell further increases, which results in a decrease of the fluorescence intensity. Figure 2d shows the corresponding UV–Vis absorption spectra of the as-synthesized ZnSe/ZnS QDs under various refluxing times. The absorption peak shows a slight red-shift in emission due to the growth of the ZnS shells, which is consistent with the PL spectra.

3.2 Structural characterization and optical properties

3.2.1 Micromorphology structure

XRD was used to examined the as-prepared QDs. Figure 3a shows the XRD patterns of the ZnSe and the optimized core–shell ZnSe/ZnS QDs, where the molar ratios of ZnSe/thiourea was 1:5, the pH was approximately 8.5 and the growth temperature and refluxing time were fixed at 90 °C and 3 h, respectively. For the ZnSe QDs, three peaks at 27.5°, 45.6° and 54.1° that relate to the diffraction from the (111), (220) and (311) crystal planes are observed, indicating that the as-prepared ZnSe QDs have cubic sphalerite structures. The XRD pattern of the
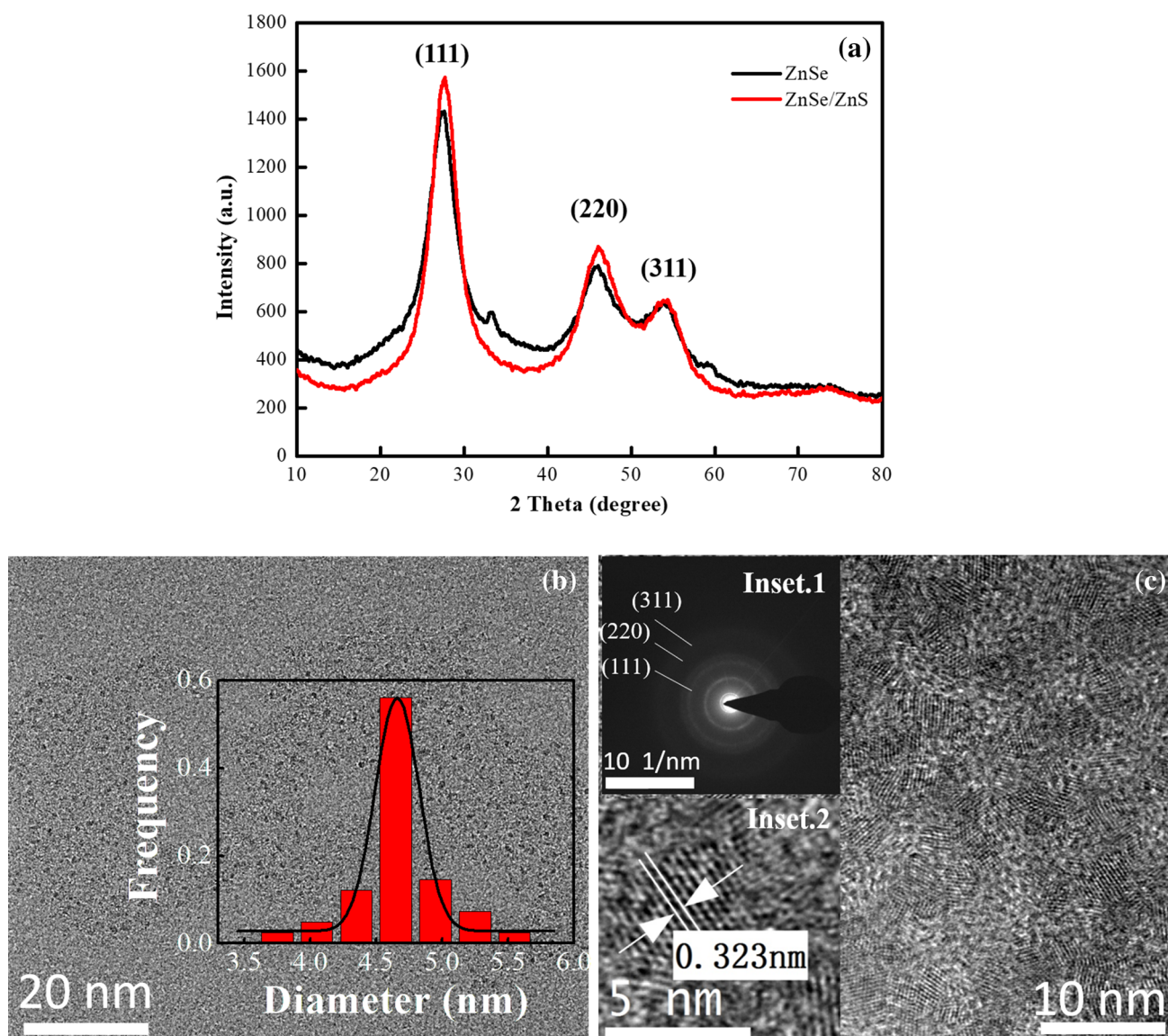
Fig. 3 **a** XRD patterns of the initial ZnSe and ZnSe/ZnS QDs. **b** TEM image of core–shell ZnSe/ZnS QDs; the inset is the particle size distribution histogram; and **c** HRTEM image of the core–shell ZnSe/ ZnS QDs. Inset.1 is the selected area electron diffraction (SAED) pattern and Inset.2 is a high-magnification pattern

core–shell ZnSe/ZnS QDs has a similar pattern as that of the ZnSe QDs without any extra peaks, but the diffraction peaks are slightly moved to higher angles. This behaviour can be explained using the Bragg equation [29]:

$$2d \sin \theta = n\lambda \tag{1}$$

where d is the interplanar space, θ is the diffraction angle, n is a positive integer, and λ is the X-ray wavelength (0.154 nm). The growth of the ZnS shells decreased the lattice parameters of the ZnSe QDs. Therefore, the diffraction peaks shift to higher angles due to the shrinkage of the core structure [30].

Figure 3b shows the TEM image of the core–shell ZnSe/ ZnS QDs, and the inset in Fig. 3b reveals the particle size distribution histogram. The results indicate that the ZnSe/ ZnS QDs have very good monodispersity and that their average diameter is approximately 4.6 ± 0.2 nm, which is an increase of 0.5 nm compared to that of the ZnSe QDs [24]. The increase in the nanoparticle size is due to the formation of the ZnS shells. This result corresponds to the red-shift of the absorption and fluorescence emission spectra of the nanoparticles, providing evidence for the formation of a core–shell structure. HRTEM further shows that the

core–shell ZnSe/ZnS QDs with a nearly spherical shape have a high degree of monodispersity and uniformity, as shown in Fig. 3c. The lattice stripes on the surface of the ZnSe/ZnS QDs with a good crystallinity could be clearly observed. The inset 1 in Fig. 3c is a selected area electron diffraction (SAED) diagram of the ZnSe/ZnS QDs and depicts three concentric rings corresponding to the (111), (220) and (311) orientations of the cubic ZnSe/ZnS QDs. Inset 2 in Fig. 3c shows that the distance between the adjacent lattices fringes are at approximately 3.22 Å, which is basically consistent with the (111) plane of a cubic zinc blende ZnSe/ZnS structure and also agrees with the XRD result.

The growth of ZnS shells around the ZnSe cores was further demonstrated by the XPS measurement results, as shown in Fig. 4a. The high-resolution Zn-2p, Se-3d and S-2p XPS spectra of the ZnSe/ZnS core–shell QDs are presented in Fig. 4b–d. The Zn core-level spectrum in Fig. 4b has been split into Zn-2p$_{3/2}$ (1022.2 eV) and Zn-2p$_{1/2}$ (1045.3 eV) with a spin–orbit splitting energy of ∼ 23.1 eV, which corresponds to that of Zn^{2+}. The Se-3d core level spectrum

in Fig. 4c is deconvoluted into two Gaussian components located at 53.3 eV (3d$_{5/2}$) and 54.2 eV (3d$_{3/2}$) with an energy splitting of 0.9 eV, implying that the chemical state of Se element is −2. The deconvoluted core-level spectrum of S-2p is shown in Fig. 4d. The bivalent S^{2-} state is confirmed by peaks at 162.1 eV (2p$_{1/2}$) and 160.9 eV (2p$_{3/2}$) with its characteristic peak separation of 1.2 eV. The S-2p peak located at 160.9 eV is attributed to the Zn–S bond. With the deposition of the ZnS shells, the percentages of the Zn and S contents increase with the thickening of the ZnS shells. These results further indicate the uniform growth of ZnS shells on the ZnSe core QDs.

To further investigate the particle size distribution and stability of ZnSe/ZnS QDs, the Zeta Potential and Nano Particle Analyzer (NanoPlus 3) was employed to measure the particle size and zeta potential distribution, where Nano particle size analyzer used Dynamic Light Scattering (DLS) method to test particle size. This technique is a common technique for determining particle size in colloidal suspensions. Particles suspended in a liquid solvent undergo
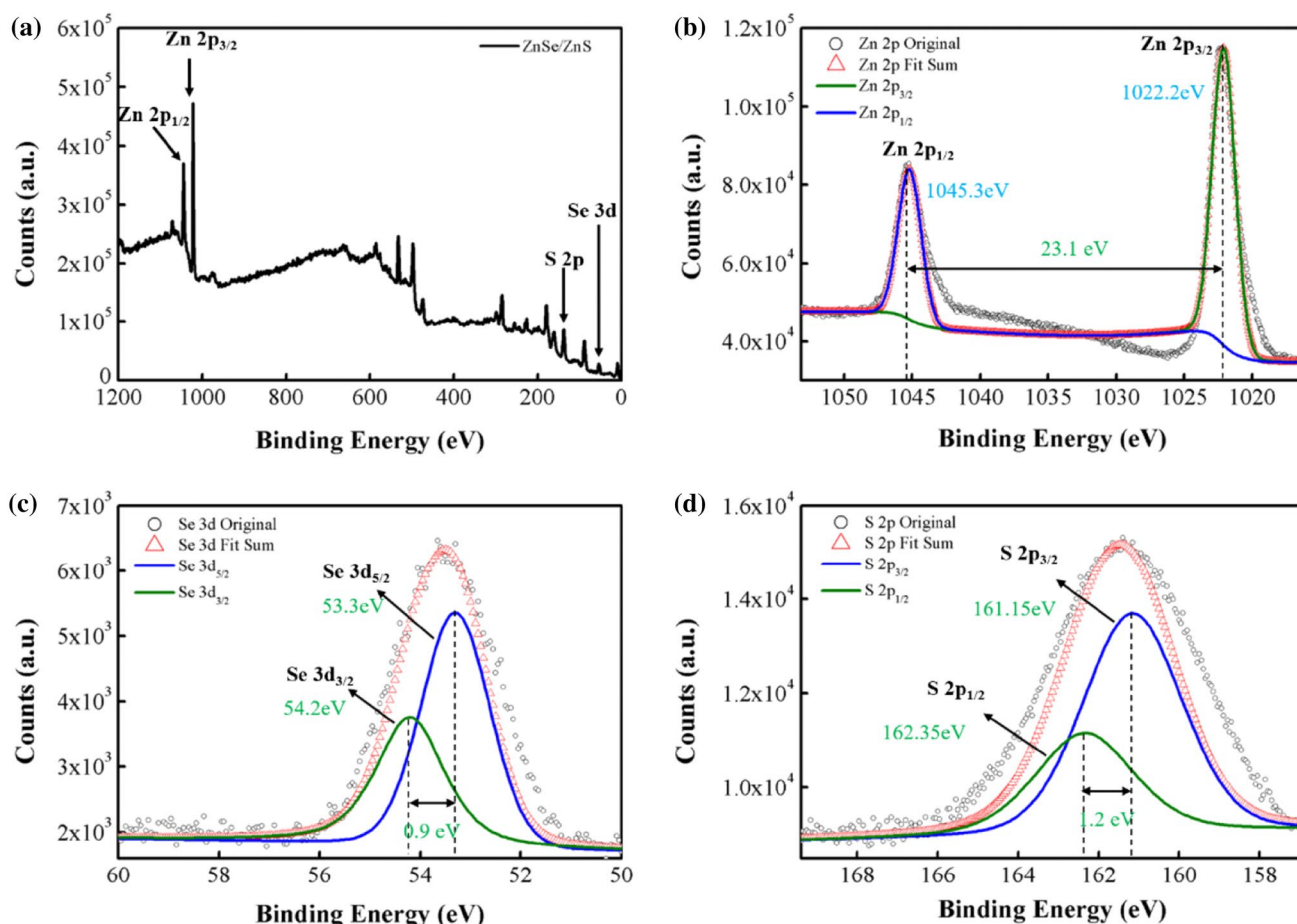
Fig. 4 **a** XPS spectrum of the core–shell ZnSe/ZnS QDs; **b** the XPS spectrum of Zn 2p; **c** the XPS spectrum of Se 3d; and **d** the XPS spectrum of S 2p
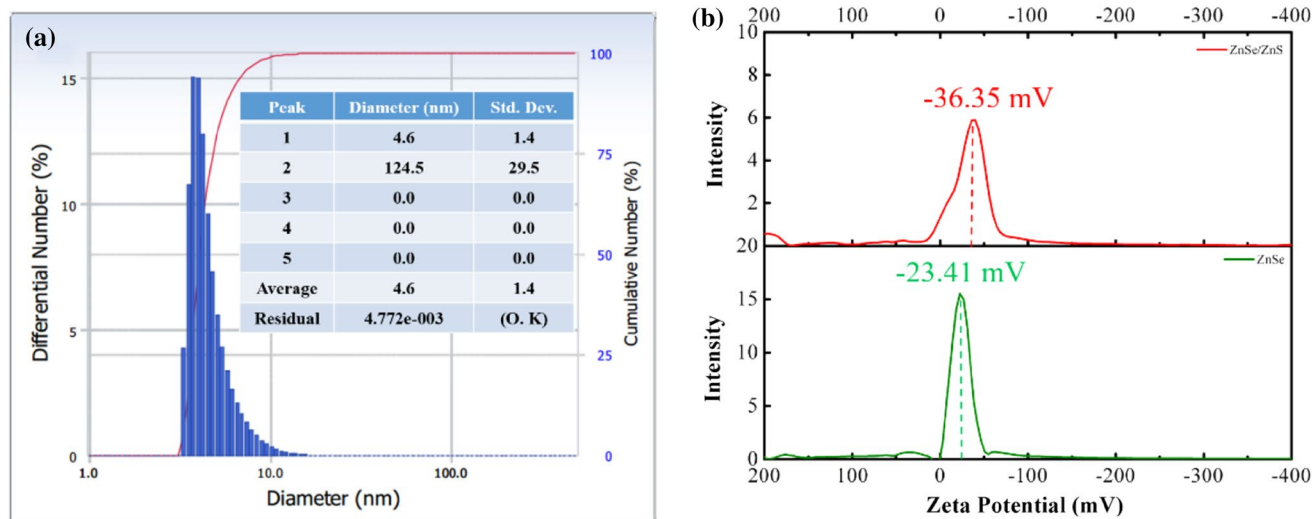
Fig. 5 **a** The particle size distribution of the core–shell ZnSe/ZnS QDs and **b** zeta potential diagrams of ZnSe and ZnSe/ZnS QDs
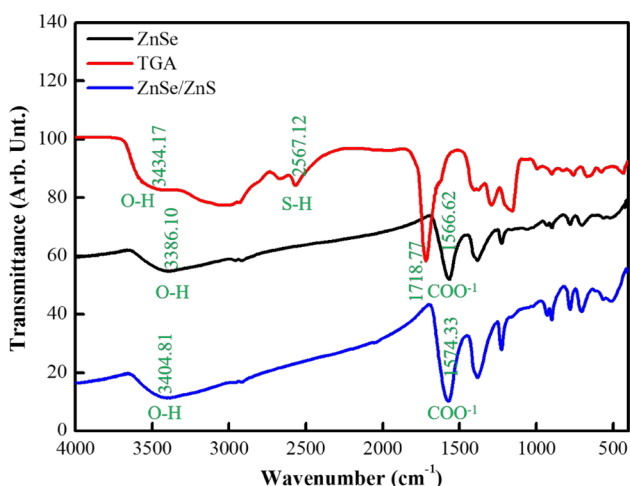
Fig. 6 FT-IR spectra of TGA, ZnSe QDs and ZnSe/ZnS QDs

random Brownian motion by a laser beam. By detecting the time-dependent fluctuations in the intensity of scattered light, an autocorrelator which determines the autocorrelation function of the signal can analyze the particle size distribution [30, 31]. Figure 5 shows the particle size and zeta potential distribution of the core–shell ZnSe/ZnS QDs. Figure 5a further confirms that the ZnSe/ZnS QDs have a good dispersibility and uniform size. The average diameter of the ZnSe/ZnS QDs is approximately 4.6 nm, which agrees well with the results of the TEM investigation. Figure 5b reveals the zeta potential distribution of the ZnSe and ZnSe/ZnS QDs. The zeta potential of the ZnSe/ZnS QDs is approximately 36.35 mV, which is much higher than that of the ZnSe QDs (23.41 mV). This result indicates that the stability of ZnSe/ZnS QDs can be better than that of ZnSe QDs.

Figure 6 presents the FI-IR spectra of the TGA and ZnSe/ZnS QDs. The important role of the TGA is to cap the QDs. There is an improved peak in the TGA spectrum at 2567 cm^{-1}, relating to the S–H bond [32, 33]. The as-synthesized QDs have no S–H stretching band between 2682 and 2561 cm^{-1}, which indicates that the S–H bond in the TGA is destroyed, a bond with the ZnSe and ZnSe/ZnS QDs surface occurred and the TGA is successfully modified on the surface of the QDs to stabilize the ZnSe and ZnSe/ZnS QDs. In these spectra, there is a broad peak between 3500 and 3000 cm^{-1} that relates to the O–H vibration of H_2O molecules; there is also a peak above 1590 cm^{-1} corresponding to the COO^{-1} asymmetric vibration [34].

3.2.2 Photostability

Figure 7a shows the absorption and PL spectra of the as-synthesized samples under the optimum condition. Compared to the ZnSe QDs, the exciton absorption peak and band edge peak of the ZnSe/ZnS QDs are approximately 377 and 402 nm, respectively. With the growth of ZnS, the absorption and band edge peaks slightly shift to longer wavelengths. Because of the formation of a core–shell structure and the increases of the particle size, the conduction band of ZnS will be located below that of ZnSe. Thus, the excited electrons in the nucleus are delocalized and the space of movement increased. These electrons are expanded to the ZnS conduction band and the emission can be attributed to the recombination of an electron in the ZnS conduction band with a hole in the ZnSe valence band, which results in a red-shift in the emission [20, 35]. The PL intensity of the ZnSe/ZnS QDs is significantly enhanced because the ZnS shell can modify the surface

(a)

(b)
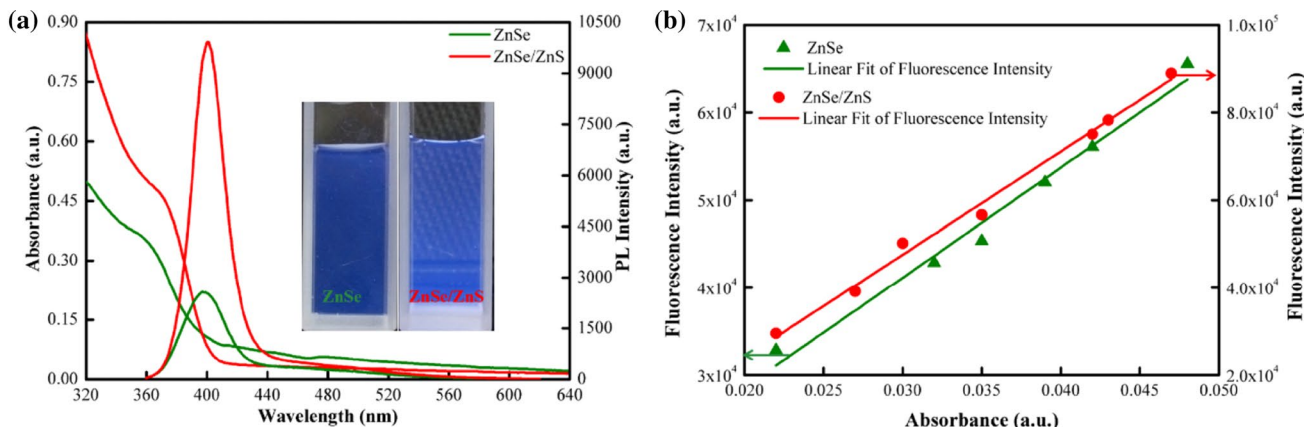
Fig. 7 **a** UV–Vis absorption and PL spectra of ZnSe QDs and ZnSe/ZnS QDs. The inset is the fluorescent image of the ZnSe QDs and ZnSe/ZnS QDs, and **b** the relationship between the integrated fluorescence intensity and absorbance

defects of the ZnSe QDs and better cap the ZnSe surface trap states [20, 36]. The inset in Fig. 7 indicates the emission images of the as-synthesized ZnSe QDs and ZnSe/ZnS QDs under UV excitation. Clearly, core–shell ZnSe/ZnS QDs are more luminous than ZnSe QDs.

As an important parameter, the fluorescence QY of the as-synthesized ZnSe/ZnS QDs is calculated by comparing the integrated fluorescence intensities (at excitations of 346 nm) and the absorbency values (at 346 nm) of QDs samples with the reference quinine sulphate. The PL QYs of the samples are calculated using the following equation [37]:

$$\Phi_X = \Phi_{XT} \left(\frac{M_x}{M_{ST}} \right) \left(\frac{n_x}{nST} \right)^2 \quad (2)$$

where the subscripts *x* and *ST* denote the QDs and reference reagent, respectively; Φ is the photoluminescence quantum yield; the *Ms* are the slopes (the gradient from the plot of the integrated fluorescence intensity versus absorbance) and *n* is the refractive index of the solvent. In this work, quinine sulphate was dissolved in 0.05 M H_2SO_4 ($\Phi = 0.55$, refractive index $n = 1.33$, $M = 2.21 \times 10^6$). The QDs samples were dissolved in deionized water (refractive index $n = 1.33$). Figure 7b reveals the relationship between the integrated fluorescence intensity and the absorbance. According to the Eq. 2 and Fig. 7b, the PL QYs of the ZnSe and ZnSe/ZnS core–shell QDs can be estimated to be approximately 31.2 and 58.5%, respectively, according to the slopes of 1.26×10^6 (ZnSe QDs) and 2.35×10^6 (ZnSe/ZnS core–shell QDs) from the plot of the integrated fluorescence intensity versus absorbance.

To further compare the optical performances of the ZnSe QDs and ZnSe/ZnS QDs, the fluorescence lifetimes of the QDs were measured. Figure 8 presents the
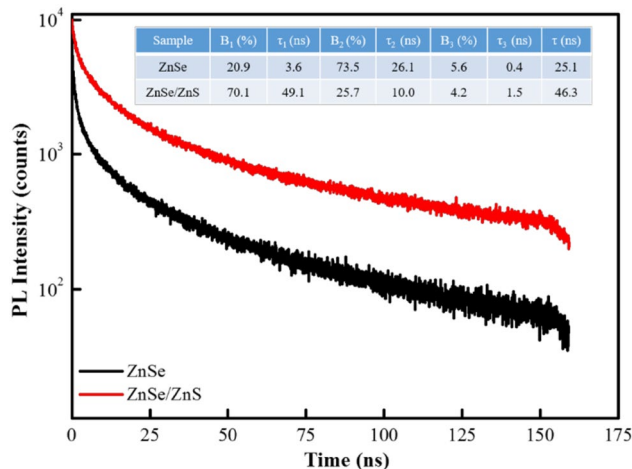
Fig. 8 Time-resolved luminescence decay curves of the ZnSe QDs and ZnSe/ZnS QDs (λex = 397 nm). The inset illustrates the detailed parameters of the ternary exponential function for each sample of as-synthesized ZnSe QDs and core–shell ZnSe/ZnS

time-resolved luminescence decay curves of the ZnSe QDs and ZnSe/ZnS QDs. In general, the PL attenuation curve for each sample is satisfactorily fitted with a ternary exponential form.

$$I(t) = A + B_1 \exp\left(-\frac{t}{\tau_1} \right) + B_2 \exp\left(-\frac{t}{\tau_2} \right) + B_3 \exp\left(-\frac{t}{\tau_3} \right)$$
(3)

where τ_1, τ_2 and τ_3 represent the time constants, B_1 and B_3 represent the amplitudes of the fast components and B_2 represents the amplitude of the slow component [24]. The time at which the PL intensity has decreased to 1/e of its initial value is used as a parameter to compare the lifetimes. The average lifetime is calculated using the following equation [38]:

$$\tau = \left(B_1\tau_1^2 + B_2\tau_2^2 + B_3\tau_3^2\right)\big/\left(B_1\tau_1 + B_2\tau_2 + B_3\tau_3\right) \qquad (4)$$

We attribute τ_1 to internal recombination. The fast component (τ_2) is contributed to surface-related recombination and the fast component (τ_3) is dominated by non-radiative recombination channels [39–41]. The inset in Fig. 8 shows the fitting parameters of different samples. Based on the results, we can obtain that the luminescence lifetime of the core–shell ZnSe/ZnS QDs is approximately 46.3 ns, which is much higher than that of the ZnSe QDs (25.1 ns). For the QD samples with higher PL QYs, the probability that the vector appears on the surface increases. The ZnS shell growth leads to the increased probability of carriers appearing on the surface, thus effectively removing the carrier quenching defect from the ZnSe surface [26].

Compared with the conventional synthesis of ZnSe/ZnS QDs, the proposed method is employed to synthesize the core/shell ZnSe/ZnS QDs at low temperature (90 °C) using a facile and green route in aqueous solution. The synthesized ZnSe/ZnS QDs with excellent blue light emission and high PL QY only consist of a band edge emission located at 398–410 nm. The excitonic emission slightly shifted to longer wavelength and the PL intensity increased considerably with the growth of ZnS shell. In the future work, we will further increase the thickness of the ZnS shell to improve the optical performance of core–shell ZnSe/ZnS QDs. On the other hand, we can also synthesize the various doped ZnSe/ZnS QDs with a wide range of emission colors using the proposed method, which is a good candidate for being used in light emitting devices, sensors, solar cells, and laser diodes.

4 Conclusion

In summary, the core–shell ZnSe/ZnS QDs with a cubic zinc blende crystalline structure were successfully synthesized using a facile and green approach. The average particle size of the ZnSe/ZnS QDs is approximately 4.6 nm. Compared with the ZnSe core, the PL intensity of the ZnSe/ZnS QDs is much stronger, and the band edge emission is slightly shifted to longer wavelengths by the growth of ZnS shell. The zeta potential of the core–shell ZnSe/ZnS QDs is approximately 36.35 mV, which is much higher than that of the ZnSe QDs (23.41 mV). The PL QY can reach 58.5%, and the exciton radiative lifetime is approximately 46.3 ns for the ZnSe/ZnS QDs. These results indicate that the as-synthesized core–shell ZnSe/ZnS QDs have an excellent stability and excellent optical properties, which have potential application value in optoelectronics and other fields.

References

1. M. Molaei, S. Pourjafari, Bull. Mater. Sci. **37**, 9–13 (2014)
2. X. Yuan, R.X. Ma, M.L. Shan, J.L. Zhao, H.B. Li, J. Lumin. **36**, 1258–1265 (2015)
3. G. Feng, C. Yang, S. Zhou, Nano Lett. **13**, 272–275 (2013)
4. F. Huang, L. Zhang, Q. Zhang, J. Hou, H. Wang, H. Wang, S. Peng, J. Liu, G. Cao, ACS Appl. Mater. Interfaces **8**, 34482–34489 (2016)
5. M.Y. Chiu, C.C. Chen, J.T. Sheu, K.H. Wei, Org. Electron. **10**, 769–774 (2009)
6. Q. Zhang, H. Li, Y. Ma, T. Zhai, Prog. Mater Sci. **83**, 472–535 (2016)
7. D. Yu, X. Zhang, Y. Qi, S. Ding, S. Cao, A. Zhu, G. Shi, Sens. Actuators B **235**, 394–400 (2016)
8. B.R. Hyun, J.J. Choi, K.L. Seyler, T. Hanrath, F.W. Wise, ACS Nano **7**, 10938–10947 (2013)
9. V.I. Klimov, A.A. Mikhailovsky, S. Xu, A. Malko, J.A. Hollingsworth, C.A. Leatherdale, H.J. Eisler, M.G. Bawendi, Science **290**, 314–317 (2000)
10. S.Z. Rahchamani, H. Rezagholipour Dizaji, M.H. Ehsani, Appl. Surf. Sci. **356**, 1096–1104 (2015)
11. Z. Fang, Y. Li, H. Zhang, X. Zhong, L. Zhu, J. Phys. Chem. C **113**, 14145–14150 (2009)
12. K.T. Yong, I. Roy, H.E. Pudavar, E.J. Bergey, K.M. Tramposch, M.T. Swihart, P.N. Prasad, Adv. Mater. **20**, 1412–1417 (2008)
13. M.A. Malik, N. Revaprasadu, P. O'Brien, Chem. Mater. **13**, 913–920 (2001)
14. P. Reiss, New J. Chem. **31**, 1843–1852 (2007)
15. M. Molaei, A.R. Khezripour, M. Karimipour, Appl. Surf. Sci. **317**, 236–240 (2014)
16. E. Soheyli, R. Sahraei, G. Nabiyouni, Opt. Mater. **60**, 564–570 (2016)
17. Y. Wang, C. Wang, S. Xu, Z. Wang, Y. Cui, Nanotechnology **25**, 295602–295609 (2014)
18. S.Z. Rahchamani, H.R. Dizaji, M.H. Ehsani, Appl. Surf. Sci. **356**, 1096–1104 (2015)
19. Z.H. Lin, M.Q. Wang, Z.L. Wei, X.H. Song, Y.H. Xue, X. Yao, J. Alloy. Compd. **509**, 8356–8359 (2011)
20. L. Ren, K.Y. Li, J.Y. Cui, T.D. Shen, J. Mater. Sci. **29**, 4478–4487 (2018)
21. M. Molaei, A.R. Khezripour, M. Karimipour, J. Lumin. **166**, 101–105 (2015)
22. B.H. Dong, L.X. Cao, G. Su, W. Liu, Communication **46**, 7331–7333 (2010)
23. Y.S. Lee, K. Nakano, H.B. Bu, D.G. Kim, Appl. Phys. Express **10**, 065001–065001 (2017)
24. L.C. He, Y.A. Zhang, S.L. Zhang, X.T. Zhou, Z.X. Lin, T.L. Guo, Mater. Technol. **33**, 205–213 (2018)
25. Z. Fang, Y. Li, H. Zhang, X.H. Zhong, L.Y. Zhu, J. Phys. Chem. C **32**, 14145–14150 (2009)
26. Z. Gu, L. Zou, Z. Fang, W. Zhu, X. Zhong, Nanotechnology **19**, 135604–135610 (2008)
27. J. Ke, X. Li, Y. Shi, Q. Zhao, X. Jiang, Nanoscale **4**, 4996–5001 (2012)
28. Y.S. Liu, Y.H. Sun, P.T. Vernier, C.H. Liang, S.Y.C. Chong, M.A. Gundersen, J. Phys. Chem. C **111**, 2872–2878 (2007)
29. K. Ou, S. Wang, G. Wan, M. Huang, Y. Zhang, L. Bai, L. Yi, J. Alloy. Compd. **726**, 707–711 (2017)
30. M.H. Christopher, S. Natasha, W. Paul, L.M. Martha, J. Nanopart. Res. **10**, 89–96 (2008)

31. K. Michael, M. David, T.C. Malcolm, K.M. Fraser, U. Nobbmann, J. Nanopart. Res. **10**, 823–829 (2008)

32. F. Dehghan, M. Molaei, F. Amirian, M. Karimipour, A.R. Bahador, Mater. Chem. Phys. **206**, 76–84 (2018)

33. A.E. Vikraman, A.R. Jose, M. Jacob, K.G. Kumar, Anal. Methods **7**, 6791–6798 (2015)

34. K. Saikia, P. Deb, E. Kalita, Curr. Appl. Phys. **13**, 925–990 (2013)

35. M.J. Murcia, D.L. Shaw, H. Woodruff, C.A. Naumann, B.A.Y. And, E.C. Long, Chem. Mater. **18**, 2219–2225 (2006)

36. X. Peng, M.C. Schlamp, A.V. K, A.P. Alivisatos, J. Am. Chem. Soc. **119**, 7019–7029 (1997)

37. C. Shu, B. Huang, X. Chen, Y. Wang, X. Li, L. Ding, W. Zhong, Spectrochim. Acta A **104**, 143–149 (2013)

38. P. Yang, N. Murase, Adv. Funct. Mater. **20**, 1258–1265 (2010)

39. J.K. Cooper, S. Gul, S.A. Lindley, J. Yano, J.Z. Zhang, ACS Appl. Mater. Interfaces **7**, 10055–10066 (2015)

40. Q. Zeng, X. Kong, Y. Sun, Y. Zhang, L. Tu, J. Zhao, H. Zhang, J. Phys. Chem. C **112**, 8587–8593 (2008)

41. X.Y. Zhang, Y. Zhang, Y. Wang, S. Kalytchuk, S.V. Kershaw, Y.H. Wang, P. Wang, T.Q. Zhang, Y. Zhao, H.Z. Zhang, T. Cui, Y.D. Wang, J. Zhao, W.W. Yu, A.L. Rogach, ACS Nano **7**, 11234–11241 (2013)